Simulations of the Tropical Intraseasonal Oscillation by the Atmospheric General Circulation Model of the Beijing Climate Center*

DONG Min (董 敏), WU Tongwen† (吴统文), WANG Zaizhi (王在志), and ZHANG Fang (张 芳)

Laboratory for Climate Studies of CMA, National Climate Center, Beijing 100081

(Received May 12, 2010)

ABSTRACT

The performance of BCC (Beijing Climate Center) AGCM 2.0.1 (Atmospheric General Circulation Model version 2.0.1) in simulating the tropical intraseasonal oscillation (TIO) is examined in this paper. The simulations are validated against observation and compared with the NCAR CAM3 (Community Atmosphere Model version 3) results. The BCC AGCM2.0.1 is developed based on the original BCC AGCM (version 1) and NCAR CAM3. New reference atmosphere and reference pressure are introduced into the model. Therefore, the original prognostic variables of temperature and surface pressure become their departures from the reference atmosphere. A new Zhang-McFarlane convective parameterization scheme is incorporated into the model with a few modifications. Other modifications include those in the boundary layer process and snow cover calculation.

All simulations are run for 52 yr from 1949 to 2001 under the lower boundary conditions of observed monthly SST. The TIOs from the model are analyzed. The comparison shows that the NCAR CAM3 has a poor ability in simulating the TIO. The simulated strength of the TIO is very weak. The energy of the eastward moving waves is similar to that of the westward moving waves in CAM3. While in observation the former is much larger than the latter. The seasonal variation and spatial distribution of the TIO produced by CAM3 are also much different from the observation. The ability of the BCC AGCM2.0.1 in simulating the TIO is significantly better. The simulated TIO is evident. The strength of the TIO produced by the BCC AGCM2.0.1 is close to the observation. The energy of eastward moving waves is much stronger than that of the westward moving waves, which is consistent with the observation. There is no significant difference in the seasonal variation and spatial distribution of the TIO between the BCC model simulation and the observation. In general, the BCC model performs better than CAM3 in simulating the TIO.

Key words: Beijing Climate Center (BCC), atmospheric general circulation model (AGCM), tropical intraseasonal oscillation (TIO), simulation study

Citation: Dong Min, Wu Tongwen, Wang Zaizhi, et al., 2010: Simulations of the tropical intraseasonal oscillation by the atmospheric general circulation model of the Beijing Climate Center. *Acta Meteor. Sinica*, **24**(5), 571–583.

1. Introduction

With the development of meteorology and climatology and the progress of computer technology, numerical prediction models have advanced rapidly in recent years. The climate components, such as atmosphere, hydrosphere (ocean, sea ice, river, and lake), geosphere, and biosphere are modeled and coupled together. The model resolutions (horizontal and vertical) are getting finer not only in the boundary layer but also in the stratosphere and middle atmosphere. Current models consider various physical, chemical, and biological processes and their interactions. Therefore, the climate model has become a complex system.

The purpose of developing a numerical climate (or general circulation) model is to build a tool to reproduce the current weather and climate realistically, and then to investigate the formation and variation mechanism of the weather or climate, and ultimately to project or even forecast the weather and climate change. A key point in model development is to validate the abilities of the model in simulating the fundamental features of real weather and climate. Through the "develop-validate-improve" approach, the climate

*Supported by the Key Basic Research Project of the National "973" Program of China under Grant No. 2010CB951902.
†Corresponding author: twwu@cma.gov.cn.
(Chinese version published in Vol. 67, No. 6, 912–922, 2009)

system model will develop continuously.

The Beijing Climate Center (BCC, also known as National Climate Center in China) is developing its own new generation climate model. The model validation is one of its major tasks. The validation of the model in simulating the basic climate state will be given in other papers. In this paper, we focus on the simulation of the intraseasonal oscillation. The tropical intraseasonal oscillation (TIO), discovered by Madden and Julian in 1971 (often referred to as Madden-Julian oscillation, MJO), is a prominent mode of the tropical atmosphere. It is associated closely with many weather and climate phenomenon in the tropics and globe (Zhang, 2005). However, simulating the TIO by global climate models is a very difficult task. Slingo et al. (1996) examined the ability of 15 models in the AMIP project in simulating the TIO, and found poor model results in this regard. Sperber et al. (1997) also showed that the ability of models in simulating the TIO is limited for most of models. Recent studies indicate that the abilities of some models in simulating the TIO have improved significantly (Inness et al., 2003; Liu et al., 2005; Zhang et al., 2006). However, there are large differences between various models.

In Section 2, a brief introduction of the BCC model is given, together with descriptions of the data and methods. The validation against the observation is provided in Section 3. A summary and discussion are presented in Section 4.

2. Model, data, and methods

2.1 Model

The new generation model of BCC (BCC AGCM2.0.1) is developed based on the original BCC model (version 1) and the NCAR CAM3 (Community Atmosphere Model, version 3) (Collins et al., 2004). The main dynamical framework and physical processes are described by Wu et al. (2008, 2010). Major modifications are as follows:

a) A new reference atmosphere and reference pressure are introduced into the model. Therefore, the original prognostic variables of temperature and surface pressure become their departures from the reference atmosphere.

b) A new Zhang-Mcfarlane convective parameterization scheme (Zhang and Mu, 2005) is incorporated into the model with a few modifications. The boundary layer process is also modified.

c) The dry convective adjustment scheme of Yan (1987) is adopted.

d) A new scheme of snow cover calculation of Wu and Wu (2004) is employed.

e) In consideration of the large influence of wind speed on the calculation of latent heating over ocean, a new latent heating calculation method is used.

2.2 Model runs

The BCC model is run from September 1949 to October 2001 under the boundary conditions of observed monthly sea surface temperature (SST). The NCAR CAM3 is also run for the same period under the same conditions.

2.3 Data and methods

Daily data are produced by the above two models. In order to reduce the data amount, the daily output is processed to generate pentad data. The ECMWF, NCEP, and CMAP (Xie and Arkin, 1997) data are used as observations to validate the model results. The time span of the ECMWF and NCEP data is from 1958 to 2000, while that of the CMAP is from 1979 to 2000.

The main methods of validation in this paper include the space-time spectral analysis with two dimensional FFT (Fast Fourier Transform), wave filtering and reconstruction, variance analysis, and wavelet analysis. The details of these methods will be given in later sections.

3. Results

3.1 Spectral structure of the simulated results

Figure 1 gives the space-time spectrum of averaged zonal wind at 850 hPa between 10°N and 10°S. This spectrum is calculated by the following procedure. Take all the zonal wind (u) values at each longitude point along a latitude for each year and form a data matrix. Its dimensions are the longitude number (128 for model grid data and 144 for NCEP or

ECMWF grid data) multiplied by day number of each year (365). First, the Fourier transform is conducted using the data at each latitude circle to obtain the spatial Fourier coefficient in each year. Then, by conducting the Fourier transform using the above Fourier coefficients in temporal direction, we obtain the two dimensional space-time Fourier coefficients for each latitude and year. The squared Fourier coefficient is the space-time spectral energy. These results are averaged between 10°N and 10°S and averaged for years. Fina-

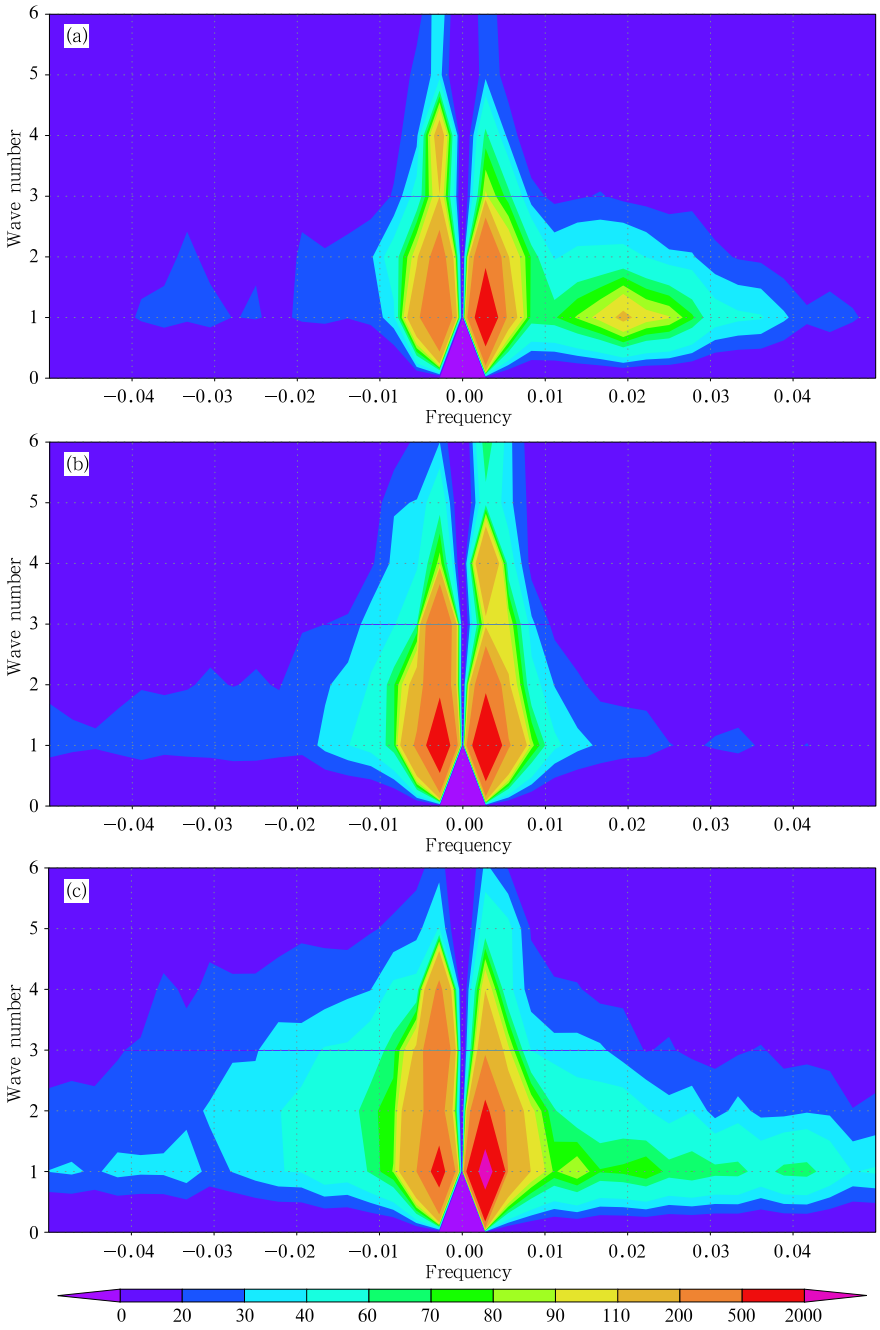

Fig. 1. The averaged time-space spectra of zonal wind u at 850 hPa in the tropical region (10°S–10°N) from the (a) ECMWF data, (b) CAM3, and (c) BCC model results. Positive frequency means the waves propagate eastward and negative frequency means the waves propagate westward. Color shadings denote the spectral power for each wave number and frequency.

lly, we obtain the climatic space-time spectrum of 850-hPa u wind in the tropical region. Figure 1a shows the result from the ECMWF. Figures 1b and 1c are from CAM3 and BCC models, respectively. The results from NCEP are almost the same as those from ECMWF (figure omitted). Figure 1a shows that the energy center is in the area where frequency is slightly greater than 0.02 with wave number being 1 for ECMWF data, i.e., the wave with the period of 42–50 days has the maximum energy.

Figure 1b shows that the energy of space-time spectrum concentrates mainly in very low frequency parts for CAM3. The energy corresponding to the frequency of intraseasonal oscillation is very weak. Moreover, in the intraseasonal frequency band the energy of westward moving waves seems slightly larger than that of eastward moving waves. Therefore, CAM3 basically cannot simulate the observed intraseasonal oscillation. Though the spectral structure of the BCC model (Fig. 1c) still bears some differences with the observation, there are great improvements compared with the CAM3. The main energy centers are distributed at wave number of 1 and frequencies of 0.013, 0.022, 0.0275, 0.033, and 0.04, i.e., there are large-scale oscillations with periods of 77, 45, 36, 30, and 25 days in the BCC model. The strongest intraseasonal oscillation has a 77-day period, which is a little longer than the observed main intraseasonal oscillation. There are also some oscillations with shorter periods. In the BCC model simulation, the waves with 50–60-day periods are weaker than observation, while the waves with periods of 70–90 and 20–30 days are slightly stronger than observation. It is notable that the energy of eastward travelling waves is larger than that of westward waves. This is consistent with the observation, and only the energy difference between eastward and westward waves is smaller than observation, i.e., in the simulation result, the westward traveling wave possesses stronger intensity. Since any two waves with the same amplitude, wave number, and frequency but opposite frequency signs can form a standing wave, there are more standing wave components in the simulation than in observation. This is another shortcoming of the model.

Figure 2 gives the space-time spectrums of precipitation for CMAP data and CAM3 and BCC models. The observational CMAP data have a pentad time resolution. Figure 2a is calculated based on the pentad precipitation data. To compare with observation, the same time resolution and same period are used for CAM3 and BCC model outputs.

From Fig. 2a, it can be seen that the precipitation has a maximum spectrum center at wave number of 1 and frequency of 0.1. Since the sampling interval of CMAP data is pentad (5 days), frequency of 0.1 corresponds to period of 50 days. Figure 2a shows that there is also relatively large energy in waves 2–3 and intraseasonal oscillation. Figure 2b shows that there is basically no intraseasonal oscillation for the CAM3 simulation. Figure 2c indicates the BCC model produces intraseasonal oscillation, but its strength is weaker than observation. In addition, the energy of the eastward moving wave is greater than that of the westward moving wave in the BCC model. This is consistent with the observation. However, since there are sizeable energy at the frequency of –0.1, the difference between eastward and westward moving waves is smaller than observation.

3.2 Geographical distribution of the TIO

Using the observational and model output pentad data, we conduct a two dimensional space-time spectral decomposition. Taking the waves with wave numbers of 1–5 and periods of 20–90 days to do reconstruction by using the reverse FFT, we obtain a new space-time series. Calculating the temporal variance of this series at each space point, we obtain the geographical distribution of the variance of TIO.

Figure 3a gives the geographical distribution of the variance of intraseasonal oscillation of 850-hPa zonal wind (u) from the NCEP data for each season. In winter, the intraseasonal oscillation is active in the Southern Hemisphere in the region along 10°S from the Indian Ocean to central Pacific (150°W). Its maximum centers are located around 180° and 120°E, and the maximum strength reaches 10 m^2 s^{-2} or so. In

spring, the center of the intraseasonal oscillation moves northwestward to the equatorial regions of the Indian Ocean (80°E) and West Pacific (150°E), and becomes slightly weaker. In summer, the active intraseasonal oscillation moves further northward to the region from West Asia to the ocean east to the Philippine Island. Its center is located in China-Indian Peninsula and its central strength is about 11–12 $m^2\ s^{-2}$, reaching its annual maximum. In fall, the intraseasonal oscillation becomes weaker and moves southward, i.e., it changes in the opposite direction. In addition, there is another active region of intraseasonal oscillation in the north side of the east equatorial Pacific. The intraseasonal oscillation is stronger in summer and autumn and weaker in winter and spring. But its location does not vary with seasons. The ECMWF

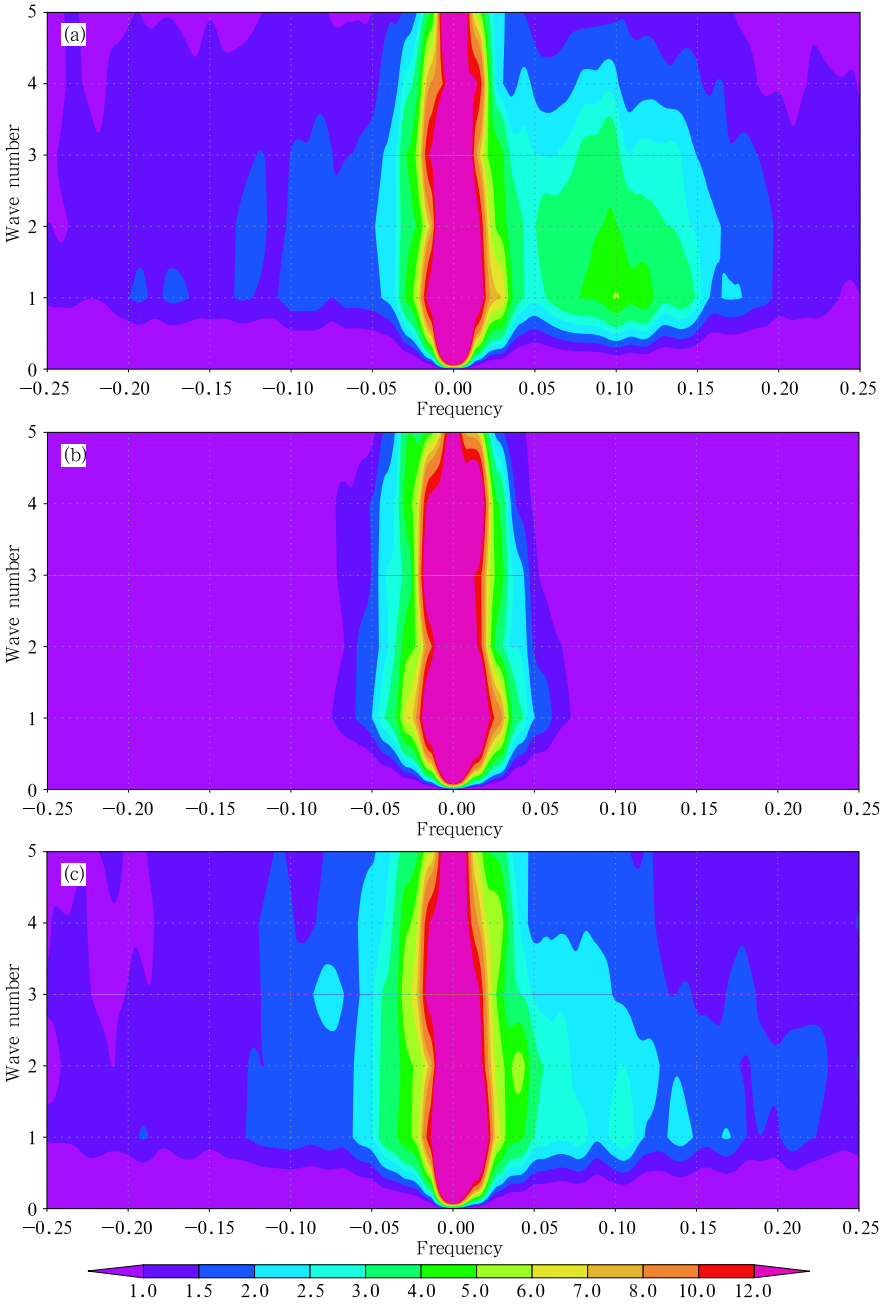

Fig. 2. The averaged time-space spectra of precipitation (pentad data) in the tropical region (10°S–10°N) from the (a) CMAP data, (b) CAM3, and (c) BCC model results.

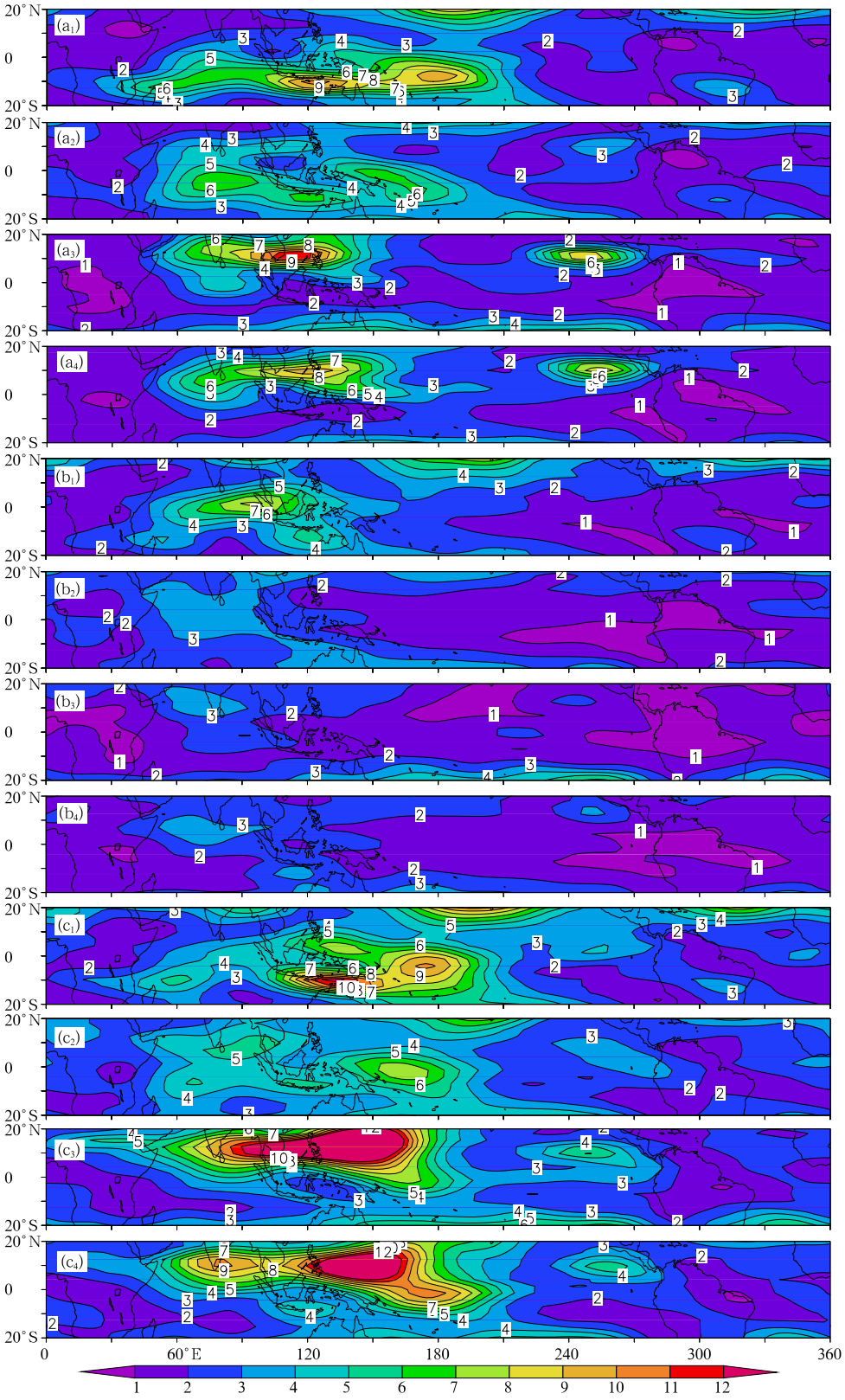

Fig. 3. The intraseasonal oscillation variance (m^2 s^{-2}) of the filtered (reconstructed) 850-hPa u wind for each season from the (a) NCEP data, (b) CAM3, and (c) BCC model results. The subscripts 1, 2, 3, and 4 denote DJF, MAM, JJA, and SON, respectively.

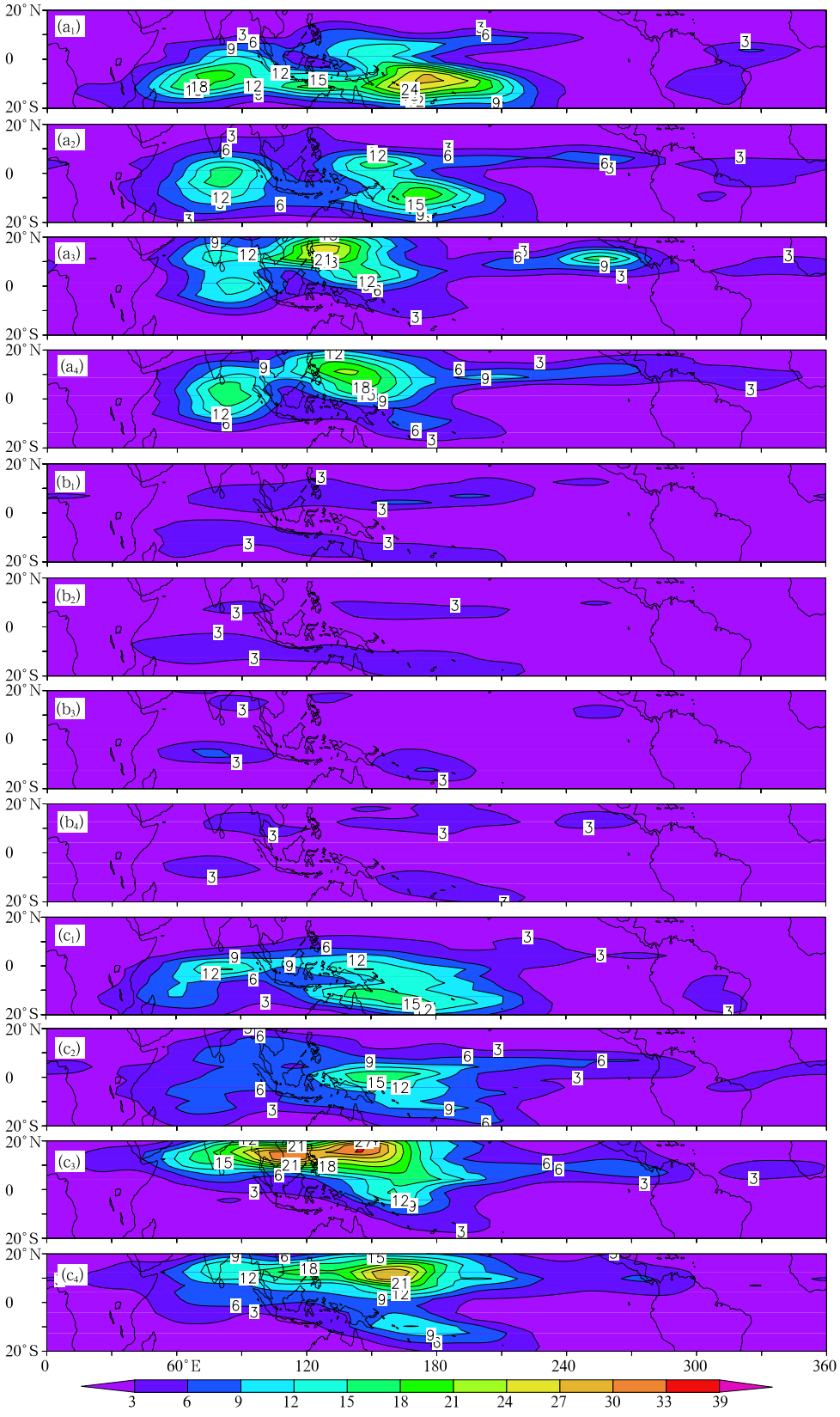

Fig. 4. As in Fig. 3, but for precipitation variance (mm^2 day^{-2}).

data show some similar results (figures omitted).

In the CAM3 simulation, the active region of intraseasonal oscillation is much different from the observation. In winter, the most active region of the intraseasonal oscillation is located over the Indian Ocean and Indonesia. Its maximum center is not in the Southern Hemisphere but near the equator. In other seasons, the intraseasonal oscillation is always weak and its active region is in the Northern Hemisphere. In the region of East Pacific north to the equator, the intraseasonal oscillation is very weak compared to observation. All of these indicate that the ability of the CAM3 in simulating the intraseasonal oscillation is very weak (Fig. 3b).

Figure 3c gives the geographical distribution of intraseasonal oscillation variance of the 850-hPa zonal wind from the BCC model. Obviously, there is much improvement compared with the CAM3 simulation results. The geographical distribution of the intraseasonal oscillation is consistent with the observation in all seasons. There are some deficiencies, for example, the intraseasonal oscillation is too strong in summer and autumn over East Asia. In the region from 90° to 150°E along 10°N, its intensity exceeds 12 m^2 s^{-2}.

Figure 4 gives the geographical distribution of the variance of intraseasonal oscillation of precipitation in all seasons for CMAP data, CAM3, and BCC model outputs. Similar to the zonal wind at 850 hPa, the variance of the intraseasonal oscillation of observed precipitation is located in the Southern Hemisphere in winter. It moves to the equatorial region in spring, and reaches the Northern Hemisphere in summer. The intraseasonal oscillation of precipitation has two relatively independent centers located in West Pacific and Indian Ocean, respectively. In addition, in north side of the equator of the East Pacific, there is also a secondary intraseasonal oscillation center, which is obvious in summer and weaker in winter and spring (Fig. 4a).

The variance of the intraseasonal oscillation of precipitation in CAM3 is very weak in all seasons (Fig. 4b). Moreover, the maximum variance centers are located over two sides of the equator and no obvious seasonal migration occurs. These features disagree with the observation.

The geographical distribution of the variance of the intraseasonal oscillation of precipitation from BCC model is close to observation (Fig. 4c). The main variance is in the Southern Hemisphere during winter and in the Northern Hemisphere during summer. Therefore, it has an obvious seasonal shift. The differences from observation are: 1) the simulated TIO over the Indian Ocean is weaker and its position is more northward than the observation; 2) in summer, the TIO in Southeast Asia is stronger than the observation; 3) the TIO in the north side of the equator of the East Pacific is weaker than the observation.

3.3 Annual cycle of the TIO

Using the Morlet wavelet, we conducted a wavelet analysis to the filtered data through the Fourier transform and the reverse Fourier transform. The temporal wavelet analysis is done at each grid point in the tropics (20°S–20°N), and the wavelet coefficients are obtained. These coefficients are functions of time and scale. In the wavelet analysis, the scale corresponds to frequency (or period) and the squared wavelet is the wave energy for a certain time or a certain period. Taking the average of energy for waves of 20–90-day periods, we obtain the energy of intraseasonal oscillation at each grid point (latitude and longitude grid) of the tropics and at each time. Since the data used are pentad data, we take the climate average of the energy for each pentad in the year. Finally, we obtain the energy of intraseasonal oscillation at each latitude and longitude grid point in the tropics and at each pentad of the year. Figure 5 displays the energy variation of the TIO with latitude or longitude during the year from observation (Fig. 5a) and two models (Figs. 5b and 5c).

Figure 5a demonstrates the variation of TIO of 850-hPa zonal wind with longitude and latitude for the NCEP data. The contour value in the upper panel is the averaged wavelet energy along the latitude from

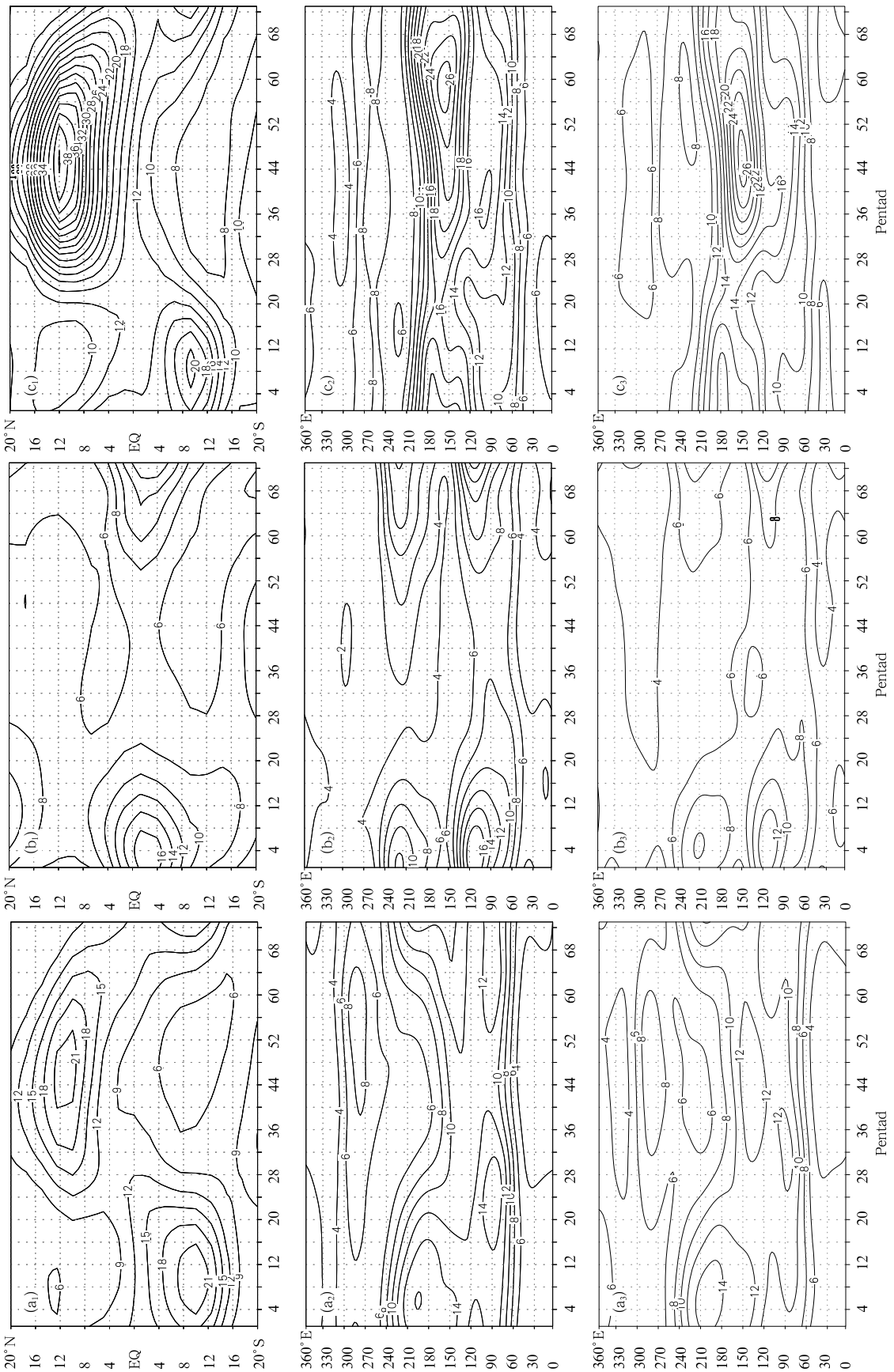

Fig. 5. The wavelet power of intraseasonal oscillation for the filtered (reconstructed) 850-hPa u wind as a function of time and longitude (or latitude). The abscissa is time (pentad of the year) and coordinates are latitude (upper panels) or longitudes (middle and lower panels). (a) NCEP data, (b) CAM3, and (c) BCC model results. (a_1,b_1,c_1) for 60°E–180°, (a_2,b_2,c_2) for 10°S–10°N, and (a_3,b_3,c_3) for 20°S–20°N.

60° to 180°E. The contour value in the middle or lower panel is the averaged wavelet energy along each longitude. The average ranges are 10°S–10°N (middle panel) and 20°S–20°N (lower panel), respectively. It is seen from Fig. 5a that the TIO in regions from the Indian Ocean to central Pacific is the strongest in winter with its value reaching 21 m^2 s^{-2}. With the seasonal transition, the TIO gets weaker, moves northward, and reaches 10°N in summer. The intensity of TIO in summer is similar to that in winter. In autumn and winter, the maximum center of TIO moves to the Southern Hemisphere again and the annual cycle ends. The middle panel of Fig. 5a shows that in the tropical central and West Pacific (10°S–10°N), the TIO is strong in winter and weak in summer, while over the Indian Ocean, the TIO is the strongest in spring. If we look at a wider region (20°S–20°N), the TIO is the strongest during spring to summer.

The TIO annual cycle of 850-hPa zonal wind from the CAM3 model differs greatly from the observation. The upper panel of Fig. 5b shows that the maximum center of TIO is in the south side of the equator in winter, then it weakens gradually and becomes the weakest in summer. Finally, it strengthens again toward winter. There is no seasonal shift from the Southern to the Northern Hemisphere. The middle and lower panels of Fig. 5b also differ greatly from observation. In winter, the TIO over the Indian Ocean is stronger than that in West Pacific and there is no significant intensification in summer.

The BCC model simulations of the annual cycle of the tropical TIO have significant improvements compared with the CAM3 simulations. From Fig. 5c, it can be seen that the tropical TIO in the region from the Indian Ocean to central Pacific is the strongest in winter with a maximum value of 20 m^2 s^{-2}. With the seasonal shift, the TIO weakens in the Southern Hemisphere, moves northward, and reaches 10°N in summer. The difference is that the TIO from the BCC model is stronger than observation in summer with a maximum value of 40 m^2 s^{-2}. From the middle and lower panels of Fig. 5c, it can also be seen that the annual cycle is captured. The deficiency of the BCC model is that the maximum center of the TIO is located westward than the observation and its maximum value is much larger than that of observation.

3.4 Propagation of the TIO

Observations indicate that the TIO travels eastward with a speed of about 5 m s^{-1}. To examine the propagation direction and speed of simulated TIO, a reference point at a certain latitude circle (e.g., the equator) is chosen. Here, we choose 0°N, 150°E as the reference point, and then calculate the lead and lag correlation between the values at reference point and the other points in the same latitude. The results are plotted in Fig. 6.

Figure 6a shows the correlation of filtered (the intraseasonal components are kept) 850-hPa zonal wind from the NCEP data. The positive correlation area has a belt shape stretching from the lower left to the upper right part of the panel. This indicates that the wind value at the west side of the reference point and that at the east side of the reference point have a good relationship with the wind value at the reference point, suggesting that the wave propagates eastward. By dividing the longitudes by the time stretched by the correlation belt, we obtain the slope of the correlation belt. From this slope, the wave propagation speed is estimated to be 5–10 m s^{-1}.

Figures 6b and 6c are the same as Fig. 6a, but for CAM3 and BCC models, respectively. It can be seen that the wave propagates westward in the CAM3 simulation and eastward in the BCC simulation. According to the slope of the correlation belt in Fig. 6c, we estimate that the traveling speed of the TIO in the BCC model is the same as that of the observation.

4. Summary and discussion

From the above analysis, it is concluded that the BCC model performs better in simulating the TIO. The improvements are as follows:

1) The BCC model simulated spectral structure is relatively closer to the observation. There is a maximum energy center at wave number of 1 and period of 20–90 days.

2) The BCC model simulated TIO has a geogra-

phical distribution consistent with the observation. The active TIO is located mainly over West Pacific and the Indian Ocean. There is also a relatively active TIO in the northern side of the equator of East

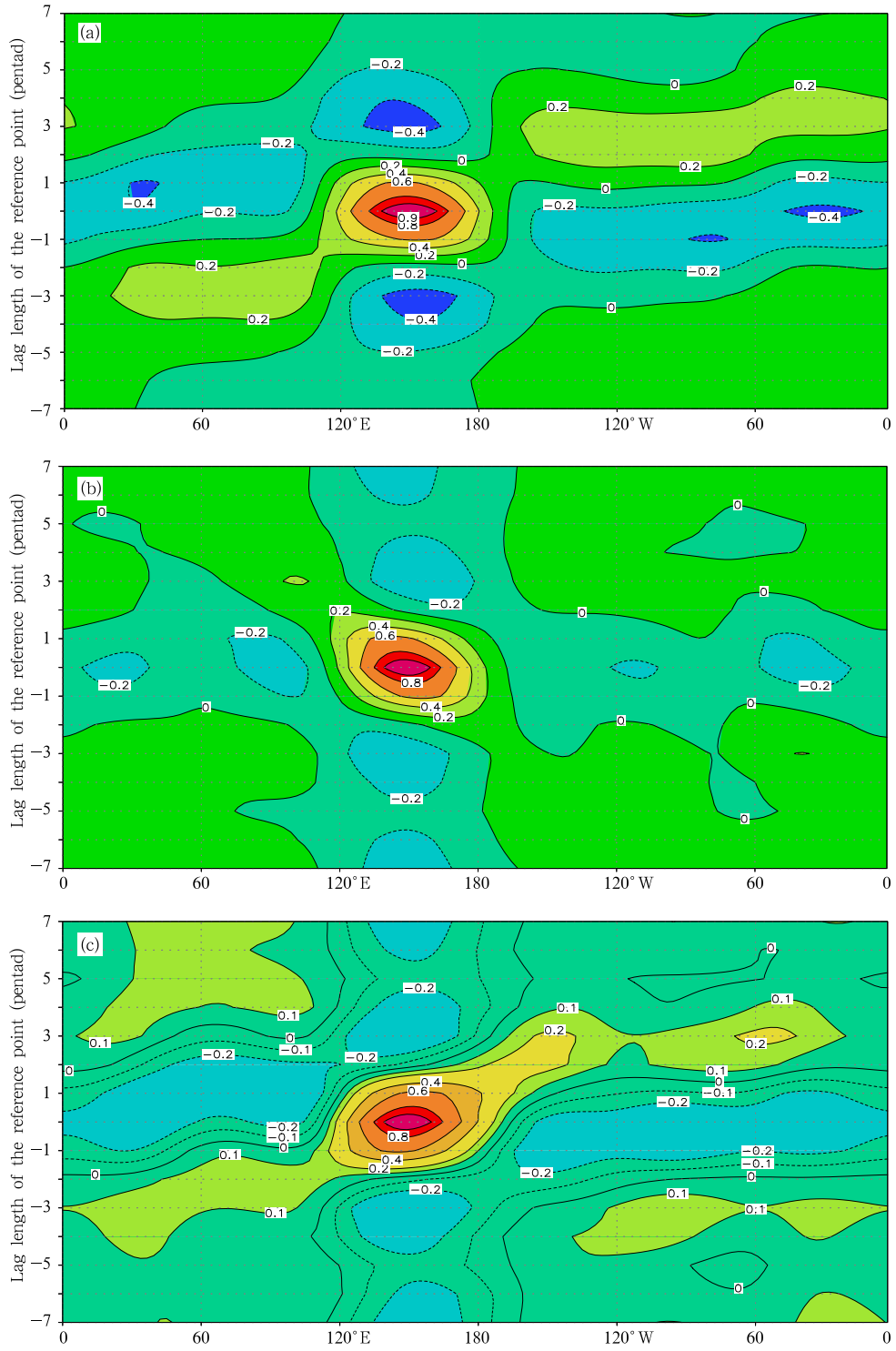

Fig. 6. The lag/lead correlation of intraseasonal component of the 850-hPa u wind at the reference point (0°N, 150°E) with the same u wind at other points along the equator from the (a) NCEP data, (b) CAM3, and (c) BCC model results. The abscissa is longitude along the equator and coordinate is the leading or lag time in pentad. Negative value means the reference point lags the other points, while positive value means reference point leads the other points.

Pacific.

3) The simulated TIO has an obvious annual cycle. Over West Pacific and the Indian Ocean, the TIO is active in the Southern Hemisphere in winter and active in the Northern Hemisphere in summer. Though there is no obvious position change for the TIO in the northern side of the equator of East Pacific during a year, the TIO shows a strength variation as being strong in summer and weak in winter.

4) The simulated TIO moves eastward and its propagation speed is basically consistent with observation.

The improvement of the BCC model in simulating the TIO may attribute to the change in the model convective parameterization. Since the changes from CAM3 to BCC exist in not only convective scheme but also many other processes, in order to test the role of convection, we conduct another experiment in which only the convection scheme is changed (we use the Zhang-Mcfarlane 2005 scheme to replace the 1995 one, which is denoted as the CAM3Z experiment) and then analyze the TIO. It is found that the CAM3Z has also attained considerable improvement in the TIO simulation. The space-time spectrum of 850-hPa u wind and precipitation for CAM3Z (figure omitted) are much like those in Figs. 1 and 2. This means that the convective scheme plays a crucial role in the TIO simulation. Of course, the BCC model simulation is better than CAM3Z, especially in capturing the annual cycle of the TIO. Though the summer TIO in Southeast Asia is still stronger than observation, it is weaker than that in the CAM3Z (figure omitted). This indicates that other improvements (e.g., the improvement in the model dynamical core) also play a certain role in the TIO simulation. Slingo et al. (1996) pointed out that if a model can well simulate the basic climate state including seasonal variation, precipitation distribution, and so on, it may have a good ability in simulating the TIO. The further improvement of the BCC model in simulating the TIO may also attribute to the improvement of overall performance of the model.

Though the BCC model can well simulate the TIO, following problems still exist:

1) The spectral energy of the BCC model results is not concentrated as in the observation. In reality, the TIO energy concentrates in 50 days or so, while in the BCC model, the TIO energy spreads over 20–90 days.

2) The westward moving component of the TIO from the BCC simulation is stronger than that in the observation.

3) The TIO of the BCC model is stronger than that in observation in West Pacific, but weaker over the Indian Ocean.

4) The TIO in summer over Southeast Asia simulated by the BCC model is too strong.

To solve these problems, we need to study the influence of the convective process on the TIO, and to find out the deficiency of the current convective scheme.

REFERENCES

Collins, W. D., P. J. Rasch, B. A. Boville, et al., 2004: Description of the NCAR Community Atmosphere Model (CAM3.0). NCAR Tech. Notes, NCAR/TN-464+STR, National Center for Atmosphere Research, Boulder, CO, USA.

Inness, P. M., J. M. Slingo, E. Guilyardi, and J. Cole, 2003: Simulation of the Madden-Julian oscillation in a coupled general circulation model. Part II: The role of the basic state. *J. Climate*, **16**, 365–382.

Liu, P., B. Wang, K. R. Sperber, T. Li, G. A. Meehl, 2005: MJO in the NCAR CAM2 with the Tiedtke convective scheme. *J. Climate*, **18**, 3007–3020.

Madden, R. A., and R. R. Julian, 1971: Detection of a 40-50-day oscillation in the zonal wind in the tropical Pacific. *J. Atmos. Sci.*, **28**(5), 702–708.

Slingo, J. M., K. R. Sperber, J. S. Boyle, et al., 1996: Intraseasonal oscillations in 15 atmospheric general circulation models: Results from an AMIP diagnostic subproject. *Clim. Dyn.*, **12**(5), 325–357.

Sperber, K. R., J. M. Slingo, P. M. Inness, and K. M. Lau, 1997: On the maintenance and initiation of the intraseasonal oscillation in the NCEP/NCAR reanalysis and the GLA and UKMO AMIP simulations. *Clim. Dyn.*, **13**, 769–795.

Wu Tongwen and Wu Guoxiong, 2004: An empirical formula to compute snow cover fraction in GCMs.

Adv. Atmos. Sci., **21**, 529–535.

——, Yu Rucong, and Zhang Fang, 2008: Modified dynamic framework for the atmospheric spectral model and its application. *J. Atmos. Sci.*, **65**(7), 2235–2253.

——, ——, ——, Zaizhi Wang, Min Dong, Lanning Wang, Xia Jin, Deliang Chen, and Laurent Li, 2010: The Beijing Climate Center atmospheric general circulation model: Description and its performance for the present-day climate. *Climate Dyn.*, **34**, 123–147, DOI 10.1007/s00382-008-0487-2.

Xie, P., and P. A. Arkin, 1997: Global precipitation: A 17-year monthly analysis based on gauge observations, satellite estimates, and numerical model outputs. *Bull. Amer. Meteor. Soc.*, **78**, 2539–2558.

Yan Hong, 1987: The design of a nested fine-mesh model over complex topography. Part II: Parameterization of sub-grid physical processes. *Plateau Meteorology*, **6**(s1), 64–139.

Zhang Chidong, 2005: Madden-Julian oscillation. *Rev. Geophys.*, **43**, RG2003, doi:10.1029/2004RG000158.

Zhang, C., M. Dong, S. Guldi, et al., 2006: Simulations of the Madden-Julian oscillation in four pairs of coupled and uncoupled global models. *Clim. Dyn.*, doi: 10.1007/s00382-006-0148-2.

Zhang, G., and M. Mu, 2005: Effects of modification to the Zhang_Mcfarlane convection parameterization on the simulation of the tropical precipitation in the National Center for Atmosphere Research Community Climate Model, Version 3. *J. Geophys. Res.*, **110**, D09109, doi:10.1029/2004JD00517.